

RESEARCH INTERESTS IN ASTROPARTICLE PHYSICS

1 The Connection Between Cluster Merger and Cosmic-ray Acceleration

When merging occurs between rich clusters of nearly equal masses, a large quantity of energy ($\sim 10^{45}$ erg/s) is released into the intracluster (hereafter IC) medium. This energy budget heats the IC gas non-uniformly mainly through weak shocks produced by the merger or turbulence that follows.

Shocks can be observed in a structured temperature map of the cluster. In Figure 1, the specific case of the merging cluster, Abell 2163, observed with the Chandra X-ray Observatory, is shown. The contours show the radio halo, which is the largest in any cluster. Shocked gas is visible to the Northeast of the cluster center.

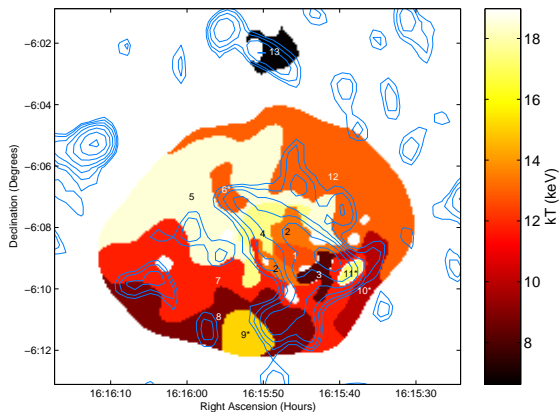


Figure 1: NVSS radio contours are shown in blue on the color-coded temperature map from Chandra observations of A2163.

When a massive cluster merger occurs and forms strong shocks in the intracluster (IC) gas, such shocks also compress the IC turbulent magnetic field and accelerate particles up to relativistic energies through the 1^{st} -order Fermi mechanism. The accelerated particles produce substantial power, $L_{CR} > 10^{44}$ erg/s, through non-thermal emission processes. The Cosmic-ray (CR) protons produce gamma-rays through $pp \rightarrow \pi^0 \rightarrow \gamma + \gamma$, and secondary electrons through $pp \rightarrow \pi^\pm \rightarrow \mu^\pm \rightarrow e^\pm + \bar{\nu}_\mu(\nu_\mu) + \nu_e(\bar{\nu}_e)$. The relativistic electrons, in turn, pro-

duce diffuse radio emission through the synchrotron process in a $\sim \mu G$ IC magnetic field and non-thermal X-rays through inverse Compton scattering (hereafter ICS) with the Cosmic Microwave Background photons. Thus, cluster mergers can produce radio halos and non-thermal, hard X-ray and γ -ray tails that are detectable with present and future observatories: the Gamma-ray Large Area Space Telescope (GLAST), the Rossi X-ray Timing Explorer (RXTE), Suzaku (X-ray), and the Giant Metrewave Radio Telescope (GMRT).

As shown below, there is a direct causal connection between the merger shock and cosmic-ray acceleration in the Abell 2163 cluster. The cosmic-rays, which produce the diffuse, non-thermal X-ray emission, were accelerated by a weak shock in the central region of the cluster, while the population of CR electrons responsible for the radio halo were accelerated by the turbulence following the shock.

If diffuse non-thermal emission (radio and/or X-ray) is due to merger shocks, the effects of these shocks should also manifest themselves in the form of temperature enhancements. Using the Rankine-Hugoniot relations we can estimate the strength of an adiabatic shock for a given temperature increase:

$$\frac{1}{r} = \left[4 \left(\frac{T_2}{T_1} - 1 \right)^2 + \frac{T_2}{T_1} \right]^{\frac{1}{2}} - 2 \left(\frac{T_2}{T_1} - 1 \right) \quad (1)$$

and

$$\mathcal{M} = \sqrt{\frac{3r}{4-r}}, \quad (2)$$

where \mathcal{M} is the Mach number, and r is the compression strength of the shock. The hottest constrained region is $kT = 18.5^{+2.7}_{-2.6}$ keV. Using this temperature, and an average cluster temperature of 12 keV, we obtain a Mach Number of $\mathcal{M} = 1.5 \pm 0.2$.

Barrowing a theoretical framework developed for Supernova shocks,

$$r \approx \frac{2\alpha_r + 3}{2\alpha_r}, \quad (3)$$

where r is defined as above, we can calculate the Mach number corresponding to the spectral index ($\alpha_r = 1.18$) of the radio halo determined by

Feretti et al. (2004, A&A, 423, 111). This gives a Mach number of $\mathcal{M} = 2.27$. On the other hand, using our best fit Photon Index ($\Gamma_X = 4.8_{-2.1}^{+1.1}$), we obtain a Mach number of $\mathcal{M} = 1.2-1.5$, consistent with the value implied by the hottest region in the Chandra temperature map. Thus, the detected shock is consistent with having produced the Inverse Compton X-ray emission but not the synchrotron radio halo.

2 Impact of Studies of Dark energy

Combining the synchrotron flux measured in the radio and the inverse-Compton flux, the magnetic field can be calculated if the spectral index is also well constrained. Dark energy measurements with galaxy clusters involves measuring the gas baryon fraction as a function of redshift. In principle, this quantity can be measured accurately by reducing counting errors with a long observation. However, systematic errors such as non-thermal pressure support are likely a significant source of uncertainty and are largely uncharacterized. Strong gravitational lensing cluster mass measurements when compared with X-ray determined mass measurements has implied a missing pressure component in the center of the cluster.

The equation of hydrostatic equilibrium, $dP/dr = -GM/r$, applied to clusters has historically only considered gas pressure ($P = P_{gas}$). However, simulations indicate that cosmic-ray protons may contribute up to 40% of gas pressure. If the magnetic field and cosmic-rays are in equipartition then magnetic field support may also be significant. Bulk flow from a recent merger may provide an additional pressure component. This means that $P = P_{cr} + P_{mag} + P_{gas} + P_{bulk}$ and all terms need to be evaluated to obtain the correct cluster mass and, hence, the baryon fraction using X-ray observations.

I've been awarded observing time (and funding) in Cycles 8,9, and 10 to observe the inverse-Compton tail in a sample of low temperature galaxy clusters with the proportional counter array (PCA: 2 - 15 keV) onboard RXTE. In a low temperature cluster, the non-thermal, power law tail will be visible beyond the exponential de-

cah of the thermal bremsstrahlung component at lower energies. Danny Hudson, University of Bonn, is a collaborator on this project. A complementary proposal has been submitted to Suzaku Cycle 1 to detect non-thermal X-ray emission from a sample hot clusters using the hard X-ray detector, which extends to higher energies where the non-thermal tail will dominate the thermal emission in hot clusters. Low frequency radio observations were awarded in cycle 7 and 9 of the GMRT (with Gopal Krishna, (NCRA,Pune).

3 Spatial Detection of Missing Baryons in Superclusters and Filaments

It may be the case that the majority of the baryonic material in the universe has not been observed. Numerical simulations suggest that in a Λ -CDM universe, a large fraction of baryons (up to $1/2$) remains in the intercluster medium, located in a hot (0.01 to 1 keV), but tenuous ($\sim \Omega_b \rho_c$) gaseous phase (Cen & Ostriker, 1999, ApJ, 514, 1). According to these same simulations, this gas is not located uniformly dispersed between the clusters of galaxies, but is located, along with the gravitationally dominant dark matter and a significant fraction ($\sim 1/4$) of the galaxy population, in web-like structures composed of filaments and, perhaps, sheets. Consequently, a large fraction of the baryon content of the universe, as inferred from primeval nucleosynthesis arguments, may yet to be observed.

The physical process that leads to filaments has been the focus of considerable attention and it has been noted that filamentary structure is present at early times in the initial density fluctuations. Alignment of tidal tensors of nearby objects produces filaments and that are therefore preferentially aligned with nearby density peaks. As a natural consequence, X-ray emission from filaments will be more common between clusters that are aligned than otherwise.

Groups are also found to be preferentially aligned with the nearest Abell clusters and are expected to be an important part of the a filamentary structure.

The Abell 3395-3391 region of the Horologium

supercluster displays an alignment of clusters and groups and the expected X-ray signature of a filament.

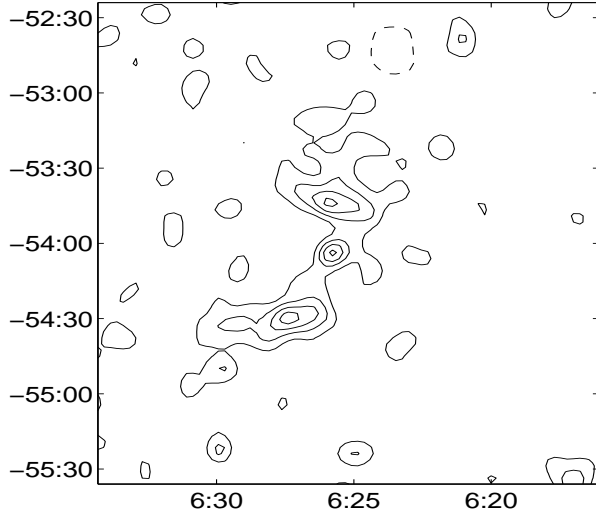


Figure 2: The galaxy sky surface density ($m_R < 15.5$) as determined from Digitized Sky Survey-II data. The contours are at levels of 2, 4, 6, ... σ above the field density.

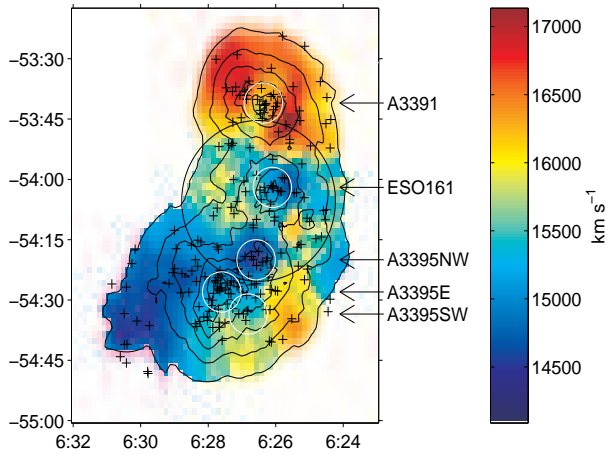


Figure 3: The galaxy concentration and mean redshifts. The sample of galaxies is indicated by the crosses. Their mean local density is given by the contour levels, which are separated by factors of two. The mean local radial velocity is illustrated by the background color scale. The larger dark circle is the *ASCA* GIS field of view.

This region is rich in optical structure. The surface number density for the galaxies in the region is given in Figure 2. Clusters A3391 and A3395 stand out, along with the galaxy group, ESO 161-G 006.

The redshift distribution among the various structures is illustrated in Figure 3. The galaxy distribution in the vicinity of A3391 and A3395 is given by the contour levels while the color axis gives the mean redshift. The cluster A3395 has $z = 0.051$ while the galaxy group lies at $z = 0.053$, midway to A3391 at $z = 0.057$.

There is an increase in the X-ray emission associated with this group of galaxies. Consequently, the cluster may be separated into three components: A3395 E, which coincides with the peak in galaxy concentration and X-ray luminosity; A3395 NW which coincides with the group of low-redshift galaxies; and A3395 SW which encompasses the second X-ray emission peak (See Figure 4). While a filament between Abell 3395-Abell 3391 was detected in the X-ray as thermal brehmsstrahlung from a hot gas at the 4σ level with the Advanced Satellite for astrophysics and cosmology, only 2% of the predicted baryons were detected. Using XMM, we will search spatially for hot baryons in the outskirts of clusters and in filaments. I am involved in two funded studies in this area: (1) Chandra observations of the Horologium supercluster (on which I am Co-I, H.Bohringer (MPE) is PI), and (2) XMM observations of the Abell 3395-Abell3391 supercluster and filament (as PI). Collaborators in this work are primarily Alexis Finoguenov and the cosmology group at MPE.

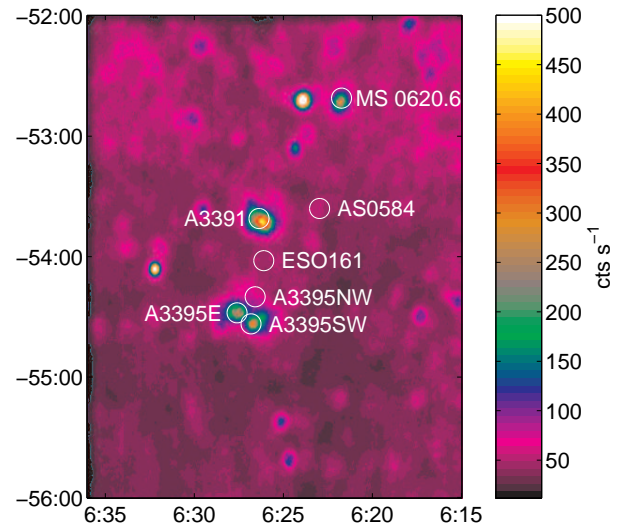


Figure 4: The field in the x-ray band from the *ROSAT* All Sky Survey.